16th Australasian Fluid Mechanics Conference
Crown Plaza, Gold Coast, Australia
2-7 December 2007

Numerical Simulation of a Blunt Airfoil Wake

C.J. Doolan

School of Mechanical Engineering
University of Adelaide, Adelaide, South Australia, 5005 AUSTRALIA

Abstract

The wake of a blunt airfoil has been analysed using a two-dimensional Unsteady Reynolds Averaged Navier Stokes (URANS) method. The $k-\varepsilon$, Spalart-Allmaras and Partially Resolved Navier Stokes (PRNS) turbulence models were compared along with experimental data. All three models were able to successfully reproduce the effect of vortex shedding on the thickness of the boundary layer at the trailing edge. However, the simulations do not show as good a comparison in the near-wake region of the airfoil, due to an over prediction of the velocity defect in all cases. The Spalart-Allmaras model provided the best prediction of the intermediate- wake region. The PRNS model persistently underestimates the centreline wake velocity in the intermediate wake.

Introduction

Solving the Unsteady Reynolds Averaged Navier Stokes (URANS) equations is attractive from a practical standpoint as it holds the promise of lower computational cost when compared with other methods, such as Large Eddy Simulation. URANS uses the same turbulence models as steady-state RANS but includes the unsteady terms in the governing equations. Lower computational cost occurs because most of the turbulence is modelled and only a small part is resolved. The difficulty with URANS is that it is theoretically ambiguous as it is not really clear how the amount of resolved and modelled turbulence is proportioned within the system of equations. Part of the problem lies in the use of the Boussinesq assumption, that assumes that the principal axes of the Reynolds stress and strain rate tensors are aligned. While this approximation may be valid for turbulent flows in equilibrium, sudden changes lead to regions of non-equilibrium turbulent flow where this assumption breaks down. Further, the dissipative nature of classical RANS turbulence models (such as the $k-\varepsilon$ model) is well known and is due to its development being based on thin shear layers such as boundary layers. Despite these shortcomings, URANS computations are becoming more popular for high Reynolds number engineering flows.

This paper will investigate the use of two-dimensional (2D) URANS with three contemporary turbulence models to compute the flow field over a blunt, 2D airfoil. Understanding the flow about blunted airfoils is important for proper control of noise and unsteady blade loading. Even small amounts of blunting [5] has been shown to cause unsteadiness about the trailing edge, affecting noise levels. Large amounts of airfoil blunting can occur in industrial applications (such as extractor fans), in specialist aeronautical applications or in wind turbines. The blunted airfoil studied here was used to generate nearly two-dimensional vortices for a fundamental vortex interaction experiment. A subsequent experimental and numerical study was performed of the blunted airfoil in isolation to obtain a more complete understanding of the vortex generation mechanisms. This paper examines these results and evaluates three turbulence models used in the numerical analysis.

The numerical results are compared with experiments and conclusions are drawn at the end of the paper regarding the suitability of URANS for unsteady wake flows.

Blunt Airfoil Experiment

Figure 1 illustrates the blunt airfoil that was used in the experiments carried out in the University of Adelaide anechoic wind tunnel [4]. The leading edge is elliptical to prevent upstream separation, therefore the only shed vorticity in the flow domain occurs at the trailing edge. The airfoil has a chord of $c = 80$ mm and a trailing edge thickness of $h = 8$ mm ($c/h = 10$). The blunt airfoil has a span of 50 mm which covers the width of the test jet exit of the anechoic wind tunnel. The wind tunnel provided a uniform test flow with a turbulence intensity of 0.37%. Additional hot-wire measurements found that that the wind tunnel wall boundary layer height was 1.5 mm for the test conditions used for this study ($U_\infty = 30$ m/s), leaving a large, uniform test core. The Reynolds number based on the trailing edge thickness was $Re_h = 16000$ and airfoil chord was $Re_c = 160000$.

Velocity measurements were obtained in the wake of the blunt airfoil using a hot-wire anemometer with a single-wire probe. These consisted of point-wise measurements that obtained the Strouhal number of the near-wake as well as wake mean velocity profiles. This information will be compared with the numerical simulations in this paper.

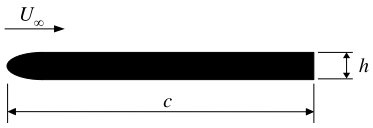

Figure 1: Illustration of blunt airfoil used in experiments

Computational Details

Computational Flow Domain

As upstream separation was suppressed using an elliptical leading edge, the main vorticity generation occurs at the trailing edge. Instead of simulating the complete flow about the blunt airfoil, a modified flow domain was used where only the flow over the trailing edge was considered. To obtain the correct boundary layer height at the trailing edge, a flat plate boundary layer solution was used. The length of the flat plate is chosen to re-create the boundary layer height expected at the trailing edge of the blunt airfoil. The expected height of the blunt airfoil boundary layer is calculated using the experimental airfoil correlations of Brooks *et al.* [1].

The correlation for *untripped* boundary layers is:

$$\frac{\delta}{c} = 10^{\left[1.6569 - 0.9045 \log Re_c + 0.0596 (\log Re_c)^2\right]} \qquad (1)$$

where δ is the boundary layer height, c is the chord and Re_c is

the Reynolds number based on the chord.

Using this correlation, the expected trailing edge boundary layer height can be calculated. Then, using standard turbulent boundary layer relations [2], an effective length of flat plate can be used to re-create the same boundary layer height. Using this method, it was determined that a flat plate of length $11.2h$ was required.

Therefore, the flow domain consists of a flat prism of length $11.2h$ and height h, where $h = 8$ mm. The flow domain is $28.7h \times 41h$ in the $x \times y$ directions, as shown in Fig. 2.

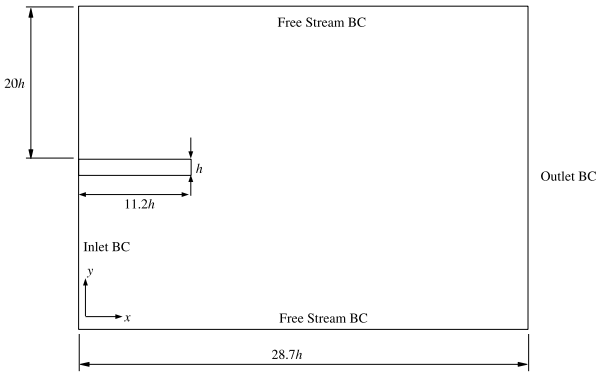

Figure 2: Flow domain used for simulations

Governing Equations and Solution Method

The unsteady Reynolds Averaged Navier Stokes (URANS) and continuity equations were numerically solved in this study. The Reynolds Averaged Equations were closed using the turbulence models describes in the next section and the Boussinesq approximation.

The equations were discretised using a structured finite-volume method [6] and the convective and diffusive terms were evaluated using a second-order accurate central-differencing method. Time integration was performed using an Euler method with the requirement that the maximum Courant number was kept below 0.2. The pressure-implicit split-operator (PISO) algorithm with two correction steps was used as an implicit, transient solution scheme. The resulting system of equations were solved using the incomplete Choleski conjugate gradient method with a solution tolerance of 10^{-6}.

Turbulence Models

Three turbulence models are considered in this study. They are the $k-\varepsilon$ model [7], the Spalart-Allmaras model [11] and the Partially Resolved Navier Stokes (PRNS) model [8].

The $k-\varepsilon$ model is a two-equation model that provides an estimate of the specific Reynolds-stress tensor via the Boussinesq approximation

$$\tau_{ij} = 2\nu_T S_{ij} - \frac{2}{3}k\delta_{ij} \tag{2}$$

where ν_T is the kinematic eddy viscosity, S_{ij} the strain-rate tensor, δ_{ij} is the Kronecker delta and k is the turbulent kinetic energy. The eddy viscosity is estimated using

$$\nu_T = C_\mu k^2/\varepsilon \tag{3}$$

Separate equations are used for the turbulent kinetic energy (k) and dissipation rate (ε) respectively

$$\frac{\partial k}{\partial t} + U_j\frac{\partial k}{\partial x_j} = \tau_{ij}\frac{\partial U_i}{\partial x_j} - \varepsilon + \frac{\partial}{\partial x_j}\left[(\nu + \nu_T/\sigma_k)\frac{\partial k}{\partial x_j}\right] \tag{4}$$

$$\frac{\partial \varepsilon}{\partial t} + U_j\frac{\partial \varepsilon}{\partial x_j} = C_{\varepsilon 1}\frac{\varepsilon}{k}\tau_{ij}\frac{\partial U_i}{\partial x_j} - C_{\varepsilon 2}\frac{\varepsilon^2}{k} + \frac{\partial}{\partial x_j}\left[(\nu + \nu_T/\sigma_\varepsilon)\frac{\partial \varepsilon}{\partial x_j}\right] \tag{5}$$

where U_i is the fluid velocity component in the i direction (with three orthogonal axes, i, j, k), t is time and x_i is the distance in the i direction. The closure coefficients are $C_{\varepsilon 1} = 1.44$, $C_{\varepsilon 2} = 1.92$, $C_\mu = 0.09$, $\sigma_k = 1.0$ and $\sigma_\varepsilon = 1.3$. Full details of the model can be found in the original reference [7].

The Spalart-Allmaras model is a one equation model that solves for the eddy viscosity of the turbulent flow. It uses the following relationship to compute the eddy viscosity

$$\nu_T = \tilde{\nu} f_{v1} \tag{6}$$

and the following equation to compute $\tilde{\nu}$ at each time step

$$\frac{\partial \tilde{\nu}}{\partial t} + U_j\frac{\partial \tilde{\nu}}{\partial x_j} = c_{b1}\tilde{S}\tilde{\nu} - c_{w1}f_w\left(\frac{\tilde{\nu}}{d}\right)^2 + \frac{1}{\sigma}\frac{\partial}{\partial x_k}\left[(\nu + \tilde{\nu})\frac{\partial \tilde{\nu}}{\partial x_k}\right] + \frac{c_{b2}}{\sigma}\frac{\partial \tilde{\nu}}{\partial x_k}\frac{\partial \tilde{\nu}}{\partial x_k} \tag{7}$$

The model requires the following closure coefficients and auxilliary relations for implementation

$$c_{b1} = 0.1355,\ c_{b2} = 0.622,\ c_{v1} = 7.1,\ \sigma = 2/3 \tag{8}$$

$$c_{w1} = \frac{c_{b1}}{\kappa^2} + \frac{1 + c_{b2}}{\sigma},\ c_{w2} = 0.3,\ \kappa = 0.41 \tag{9}$$

$$f_{v1} = \frac{\chi^3}{\chi^3 + c_{v1}^3},\quad f_{v2} = 1 - \frac{\chi}{1 + \chi f_{v1}},\quad f_w = g\left[\frac{1 + c_{w3}^6}{g^6 + c_{w3}^6}\right]^{1/6} \tag{10}$$

$$\chi = \frac{\tilde{\nu}}{\nu},\ g = r + c_{w2}(r^6 - r),\ r = \frac{\tilde{\nu}}{\tilde{S}\kappa^2 d^2} \tag{11}$$

$$\tilde{S} = S + \frac{\tilde{\nu}}{\kappa^2 d^2}f_{v2},\ S = \sqrt{2\Omega_{ij}\Omega_{ij}} \tag{12}$$

$$\Omega_{ij} = \frac{1}{2}\left(\frac{\partial U_i}{\partial x_j} - \frac{\partial U_j}{\partial x_i}\right) \tag{13}$$

where d is the distance to the closest surface. Full details of the model can be found in the original reference [11].

The $k-\varepsilon$ and Spalart-Allmaras models are well known and used for steady turbulent flows. However, their ability to capture important transient flow phenomena is limited, as their original formulations are based upon steady shear layers. Additionally, there is some ambiguity as to what scales are modelled and what scales are resolved. Large Eddy Simulation (LES) has been shown to be useful in simulating unsteady, turbulent flows with high accuracy, however, the computational requirements are high, as the method attempts to simulate the turbulent structures down to the inertial scale. In some engineering analyses,

only the important large scales of the flow need to be resolved, so there is a requirement for a new approach to enable more accurate simulations at moderate computational cost.

The PRNS method [8] is an attempt to provide a more computationally tractable method of solving unsteady turbulent flow problems. The method uses temporal filtering over a fixed time or frequency limit instead of the usual Reynolds averaging to obtain temporally filtered Navier Stokes equations. A temporally filtered variable ($\overline{\phi}$) can be calculated using a fixed temporal filter width (Δ_T) using

$$\overline{\phi}(t,x_i) = \frac{1}{\Delta_T}\int_{t-\Delta_T/2}^{t+\Delta_T/2} \phi(\tau,x_i)d\tau \qquad (14)$$

Thus, the usual Reynolds averaging occurs when $\frac{\Delta_T}{T} = \infty$ and no averaging occurs when $\frac{\Delta_T}{T} = 0$.

Temporal filtering can be applied to the Navier Stokes equations analogously to a Reynolds averaging operation. The result is a set of equations known as the Partially Averaged Navier Stokes equations. The temporal filter width can be used to control the partition between resolved and modelled turbulent scales in a way similar to the spatial filter of LES. PRNS does this through controlling the eddy viscosity with the turbulence model. For example, for the $k-\varepsilon$ model, it can be shown that the PRNS eddy viscosity is

$$\nu_T = \left(\frac{\Delta_T}{T}\right) C_1 \left(\frac{k^2}{\varepsilon}\right) \qquad (15)$$

where $C_1 = C_\mu = 0.09$, T is the global integral time scale for the flow and $\frac{\Delta_T}{T}$ is known as the *Resolution Control Parameter*. The original formulation [8] uses $\frac{\Delta_T}{T} = 0.38$, and this is the same parameter value used in this study.

Computational Mesh

The simulation described here was performed on a non-uniform Cartesian mesh. Five meshes were used to establish the accuracy of the solution method. The discretisation error based on solutions obtained from these five meshes is discussed in the **Convergence** section below. The finest grid density investigated in this study contained $N_x = 325 \times N_y = 184$ grid points and all simulation results presented in this paper use this grid.

Flow Field Initialisation

A two-dimensional potential flow solver is used to create a conservative flow field to initialise the simulations. Using this as the starting condition at $tU_\infty/h = 0$, the two-dimensional URANS equations are iteratively solved. It takes approximately 5000 time steps or a non-dimensional time of $tU_\infty/h = 18.75$ for vortex shedding to begin. All initial flow transients have disappeared by $tU_\infty/h = 150$ or 5.2 computational domain flow-through times.

Flow simulations are obtained after the initialisation period for $tU_\infty/h = 112.5$ non-dimensional time units or 4 domain flow-through times. This corresponds to 30000 time steps and captures 25 vortex shedding cycles with 1200 time steps per shedding period on the finest mesh.

Convergence

Determining the grid convergence or discretisation error is an important part of any numerical analysis. Here, three methods, based on the Richardson extrapolation [9] technique, were used to estimate the grid independent solution. Three methods were required, as it it sometimes difficult to properly estimate the order of the solution, especially in turbulent flows [10, 3].

The first and second order Richardson extrapoloation methods of Celik and Karatekin [3] were used. A special mixed-order technique [10] was also used. Including a mixed-order method was considered important because, in the current flow simulations, all spatial derivatives were approximated by second order accurate schemes, but the time integration was Euler, which is first order. Therefore, the method was regarded as mixed and the order should be realistically bounded between 1 and 2.

To estimate discretisation error, the time-varying flow velocity at a point $x = 1.75h, y = 0.75h$ from the trailing edge mid-plane was used for the analysis. Table 1 summarises the error calculated using the first, second and mixed order schemes. It can be seen that the error of the solution was below 2.8% regardless of the order assumed.

Table 1: Discretisation Error Results

Order	Error, e_h
Mixed-Order	2.34%
First-Order	2.07%
Second-Order	2.73%

Simulation Results

Instantaneous Results

Figure 3 shows colour contours of instantaneous vorticity about the trailing edge region at $tU_\infty/h = 262.5$ for all modelling techniques under investigation. In this and subsequent figures, the length scale is given by the trailing edge height $h = 8$ mm. It can be seen that a Von-Karman-like vortex street forms behind the trailing edge, due to strong, alternate shedding of the airfoil boundary layers from the top and bottom surfaces. The shedding process is complex, as it involves a redistribution of eddy length-scales from the boundary layer, where the maximum energy containing eddies have a size $l_p \sim \delta$, to the wake, where $l_p \sim h$. The unsteady nature of the wake induces fluctuating forces on the airfoil which results in radiated noise (as measured in experiments [4]).

There are small but significant differences in the instantaneous vorticity for each of the turbulence models shown here. The largest differences are in the near-wake region. The PRNS model creates vortices whose intensity persists further into the wake than the other models.

Figure 4 compares the modelled turbulent kinetic energies for the $k-\varepsilon$ and PRNS models. The SA model doesn't directly model the turbulent kinetic energy. The modellled eddy viscosity is shown as this is related to the turbulent kinetic energy through a constant and a turbulent length scale: $\nu_T = C\sqrt{k}\ell$. It can be seen that the majority of modelled turbulent kinetic energy is generated in the near-wake region. Interestingly, the PRNS method shows a finer resolution of modelled kinetic energy, allowing larger and higher frequency velocity fluctuations to be directly resolved on the grid. The Spalart-Allmaras model shows increasing eddy viscosity generation with distance behind the trailing edge.

The time history of the velocity taken at a point just behind the trailing edge at $x = 1.75h, y = 0.75h$ from the trailing edge mid-plane is shown in Fig. 5(a). It can be seen that the signal

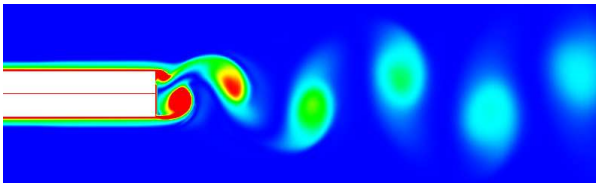

(a) Vorticity magnitude, $k-\varepsilon$

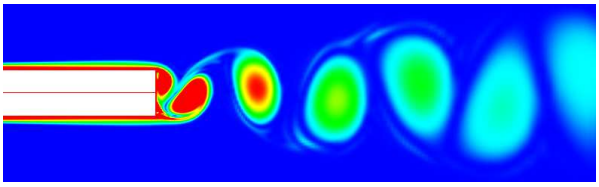

(b) Vorticity magnitude, Spalart-Allmaras

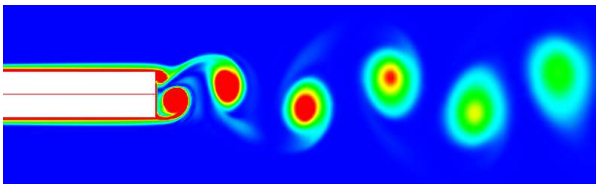

(c) Vorticity magnitude, PRNS

Figure 3: Instantaneous vorticity magnitude, contours at $tU_\infty/h = 262.5$. Contours are equally spaced over a range of $0 < \frac{\omega h}{U_\infty} < 4$

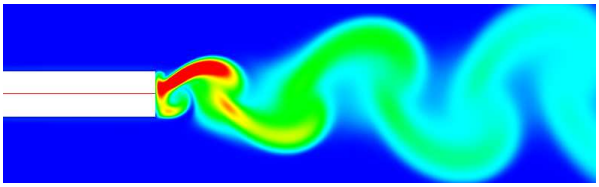

(a) Modelled turbulent kinetic energy, $k-\varepsilon$

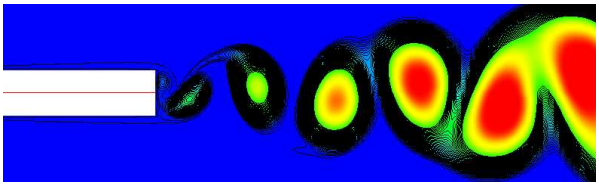

(b) Modelled eddy viscosity, Spalart-Allmaras

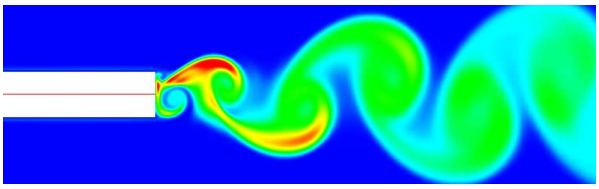

(c) Modelled turbulent kinetic energy, PRNS

Figure 4: Instantaneous modelled turbulent kinetic energy and eddy viscosity, contours at $tU_\infty/h = 262.5$. Contours are equally spaced over a range of $0 < \frac{\sqrt{k}}{U_\infty} < 0.3$ for (a) and (c). Contours are equally spaced over a range of $0 < \frac{\nu_T}{\nu} < 880$ for (b)

is periodic, with the fundamental Strouhal number varying between $f_0 h/U_\infty = 0.219 - 0.231$ for the three test cases. This is confirmed by the frequency spectra for each model, shown in Fig. 5(b-d), which was calculated using a Fast-Fourier-Transform (FFT) procedure with no pre-treatment or filtering of the numerical data. It is interesting that compared with the standard $k-\varepsilon$ model, the Spalart-Allmaras model increases the Strouhal number and PRNS reduces it, according to the the way each accounts for eddy viscosity production. Most major frequency peaks are similarly captured by each turbulence model.

The Strouhal number obtained by experiment [4] using hot-wire anemometry at the same point was found to be 0.267, much higher than the numerical simulations and other blunt airfoil studies [1], which is usually about 0.21. The reasons for such a high measured Strouhal number is unclear but maybe due to coupling between the shear layers of the free-jet wind tunnel and the shed vorticity of the airfoil.

Streamlines

Figure 6 shows streamlines computed from time averaged numerical results. The streamlines show a well-defined, symmetric recirculation region immediately behind the trailing edge in each case. The Spalart-Allmaras model increases the recirculation bubble while PRNS reduces it. To further quantify the recirculation bubble size and velocity field in the near wake, numerical centerline stremwise velocity data is shown in Fig. 7. Despite the differences in the near wake, the $k-\varepsilon$ and Spalart-Allmaras models have similar streamwise velocity in the intermediate-wake and beyond. The PRNS model, however, has a shorter recirculation bubble length, more intense recirculation within the bubble and a persistantly low centerline streamwise velocity level when compared with the other models investigated in this study.

Mean Flow Results

Figure 8 compares numerical and experimental [4] mean boundary layer velocity profiles at the location of the trailing edge for each turbulence model. For these results, $y = y^+ = 0$ indicates the surface of the trailing edge. It can be seen that, in each case, the outer regions of the boundary layer are correctly modelled when compared with experiment. Also, the technique used to simplify the flow domain is shown to be accurate as well.

In the log-layer ($10 \leq y^+ \leq 100$), each model exhibits a different response, depending on how individual wall functions are implemented. For the $k-\varepsilon$ and PRNS models, a log-layer wall function: $u^+ = 1/\kappa \ln y^+ + 9.0$ was used (where u^+ and y^+ are the friction velcocity scaled boundary layer velcoity and normal height [12]). No wall function was used for the Spalart-Allmaras model (as it uses its own wall damping function) and it can be seen that the log-layer response is quite different. In all cases, the computations show that the mean velocity level falls as y^+ is increased into the defect-layer ($y^+ > 200$), where the usual expectation is that the u^+ values will rise to reach the free stream velocity. Hence vortex shedding has the effect of increasing the thickness of the lower regions of the boundary layer and distorting the merging of the boundary layer with the free stream.

Mean velocity experimental data [4] for the wake region is also compared with numerical results in Fig. 9 at three downstream locations: $x/h = 1.75$, $x/h = 4.88$ and $x/h = 8.00$. In the near-wake region ($x/h = 1.75$), agreement is poor for all turbulence models, with the URANS results overestimating the velocity defect behind the trailing edge. In the near-wake, major flow changes are occurring and the assumption that production and dissipation are matched (as occurs in boundary layer flows) breaks down, resulting in poor comparisons with experiment.

Despite an attempt to rectify this situation by modifying the eddy viscosity, the PRNS model has poorer agreement in the near-wake. One possible reason for this is the lack of streamwise vorticity in the simulation.

At distances beyond the initial development region ($x/h = 4.88$ and $x/h = 8.00$), agreement is better in each case except for the PRNS model. PRNS underpredicts the velocity in the central region of the wake, but has reasonable prediction of the wake outside of this central zone. The $k-\varepsilon$ and Spalart-Allmaras models both have reasonable comparisons with experiment in the intermediate wake and beyond.

Conclusions

The following major conclusions can be drawn:

1. Simplifying the flow domain using an empirical airfoil boundary layer relationship has been shown to be successful for this type of flow.
2. 2D URANS can accurately model the effect of vortex shedding on the mean turbulent boundary layer profile at the trailing edge of a blunt airfoil.
3. There is a slight but significant effect on vortex shedding frequency for each turbulence model.
4. The mean velocity defect in the near-wake is significantly over-predicted using 2D URANS techniques.
5. The 2D PRNS model significantly underpredicts centreline velocity in the near and intermediate wake regions.
6. The $k-\varepsilon$ and Spalart-Allmaras models have reasonable agreement in the intermediate wake region.

As a final note, it is concluded that 2D URANS is a useful tool for studying unsteady turbulent flow physics as long as the user understands the limitations of the method and turbulence model employed. To increase the accuracy of URANS methods, more attention is required to increase the fidelity of the turbulence closure model and understanding how to control or better influence the distribution of turbulent kinetic energy between modelled and resolved components. The PRNS method attempts to do this, but it fails in this case in the near wake. There are two possible reasons for this. The first is the lack of inclusion of streamwise vorticity in the model. The second is the control over how eddy viscosity is modified. In the present study, a global resolution control parameter was employed. It can be argued, however, that $\frac{\Delta_T}{T}$ should be dependent on the grid spacing and time-step and be a function of the following form

$$\frac{\Delta_T}{T} = f\left(\frac{\sqrt{U_i^2}\delta t}{\Delta}\right) \tag{16}$$

In this way, a hybrid URANS-LES method can be developed. This method could form part of a new RANS-LES hybrid method called the Temporally Filtered Navier Stokes (TeFiNS) technique.

Acknowledgements

This work has been supported by the Sir Ross and Sir Keith Smith Fund.

References

[1] Brooks, T., Pope, D. and Marcolini, M., Airfoil self-noise and prediction, Reference Publication 1218, NASA, 1989.

[2] Cebeci, T. and Bradshaw, P., *Momentum Transfer in Boundary Layers*, McGraw Hill, 1977.

[3] Celik, I. and Karatekin, O., Numerical experiments on application of richardson extrapolation with nonuniform grids, *Journal of Fluids Engineering*, **119**, 1997, 584–590.

[4] Doolan, C. and Leclercq, D., An anechoic wind tunnel for the investigation of the main-rotor/tail-rotor blade vortex interaction, in *Proceedings of the 6th Australian Vertiflite Conference on Helicopter Technology*, American Helicopter Society International, Inc., 2007.

[5] Herr, M. and Dobrzynski, W., Experimental investigation in low-noise trailing edge design, *AIAA Journal*, **43**, 2005, 1167–1175.

[6] Jasak, H., Weller, H. and Nordin, N., In-cylinder cfd simulation using a c++ object orientated toolkit, Technical Report SAE Technical Paper 2004-01-0110, Society of Automotive Engineers, 2004.

[7] Launder, B. and Sharma, B., Application of the energy dissipation model of turbulence to the calculation of flow near a spinning disc, *Letters in Heat and Mass Transfer*, **1**, 1974, 131–138.

[8] Liu, N. and Shih, T., Turbulence modeling for very large eddy simulation, *AIAA Journal*, **44**, 2006, 687–697.

[9] Richardson, L., The approximate arithmetic solution by finite differences of physical problems involving differential equations with application to stresses in a masonry dam, *Transactions of the Royal Society of London, Series A*, **210**, 1910, 307–357.

[10] Roy, C., Grid convergence error analysis for mixed-order numerical schemes, *AIAA Journal*, **41**, 2003, 595–604.

[11] Spalart, P. and Allmaras, S., A one-equation turbulence model for aerodynamic flows, AIAA Paper 92-439.

[12] Wilcox, D., *Turbulence Modeling for CFD*, DCW Industries, La Canada, CA, USA, 2006, 3rd edition.

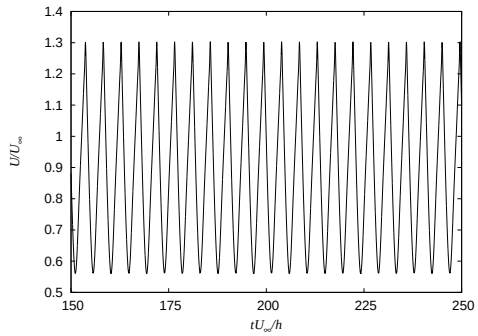

(a) Time history, $k-\varepsilon$

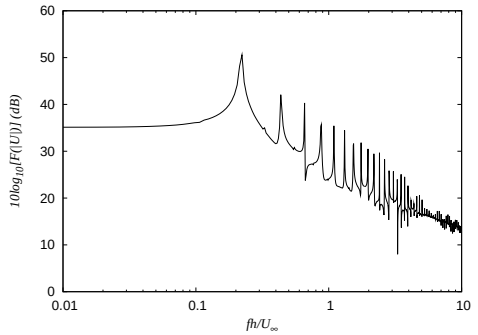

(b) Frequency spectra, $k-\varepsilon$, $f_0h/U_\infty = 0.222$

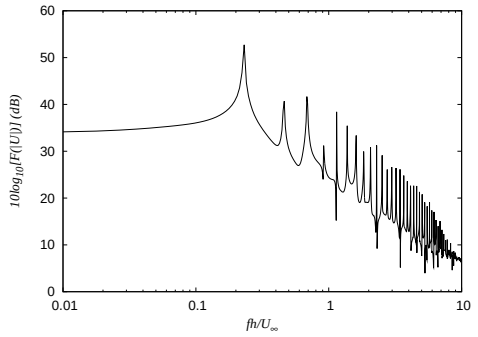

(c) Frequency spectra, Spalart-Allmaras, $f_0h/U_\infty = 0.231$

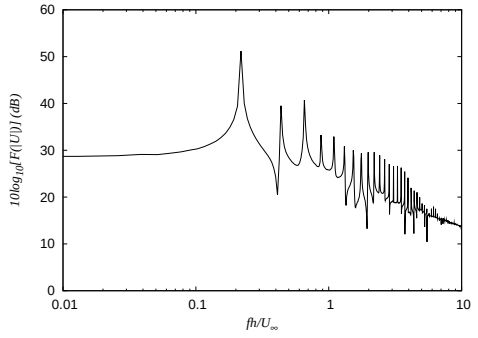

(d) Frequency spectra, PRNS, $f_0h/U_\infty = 0.219$

Figure 5: Velocity data obtained at a point $x = 1.75h, y = 0.75h$ from the trailing edge mid-plane

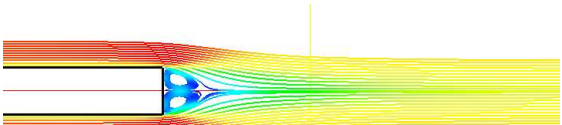

(a) $k-\varepsilon$

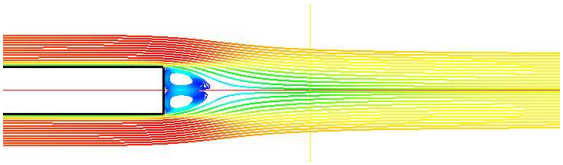

(b) Spalart-Allmaras

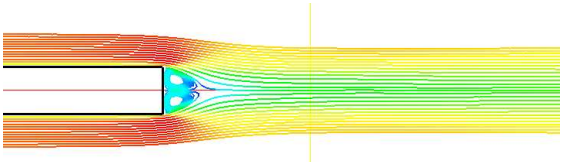

(c) PRNS

Figure 6: Streamlines in the trailing edge region. Coloured by mean velocity.

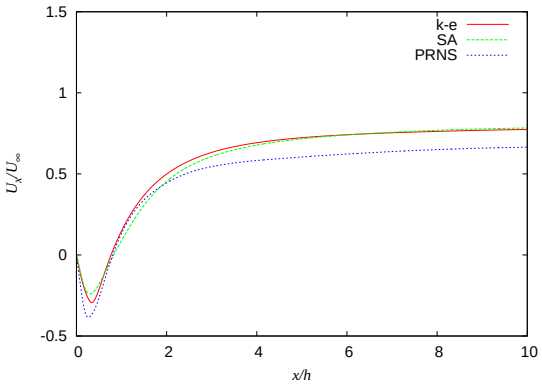

Figure 7: Streamwise velocity on the centre line of the wake. ke = $k-\varepsilon$, SA = Spalart-Allmaras and PRNS = Partially Resolved Navier Stokes.

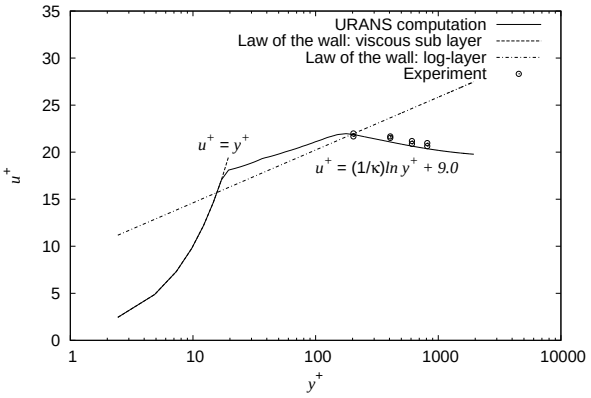

(a) $k-\varepsilon$

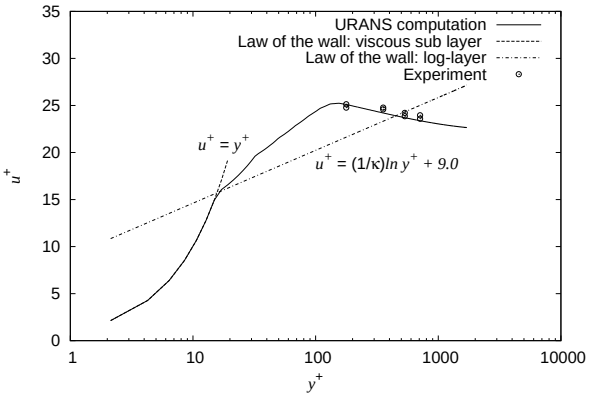

(b) Spalart-Allmaras

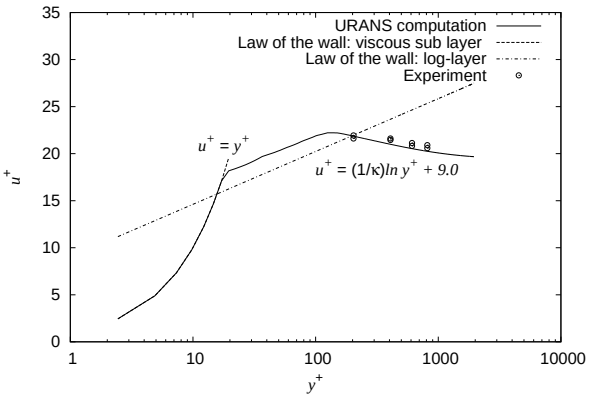

(c) PRNS

Figure 8: Comparison between time averaged URANS computation, experiment and law of the wall

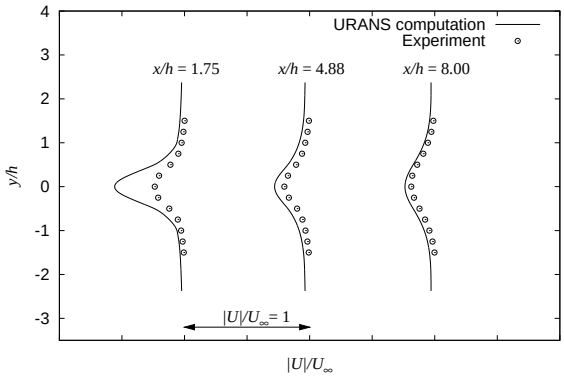

(a) $k-\varepsilon$

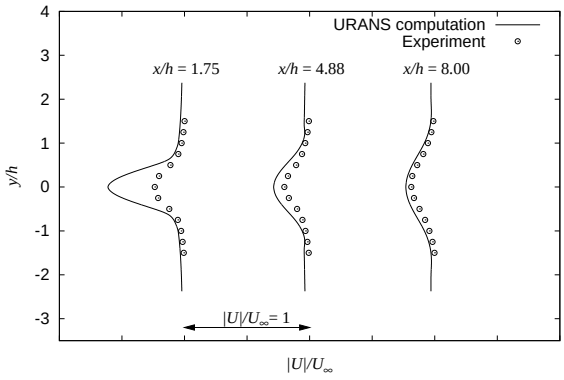

(b) Spalart-Allmaras

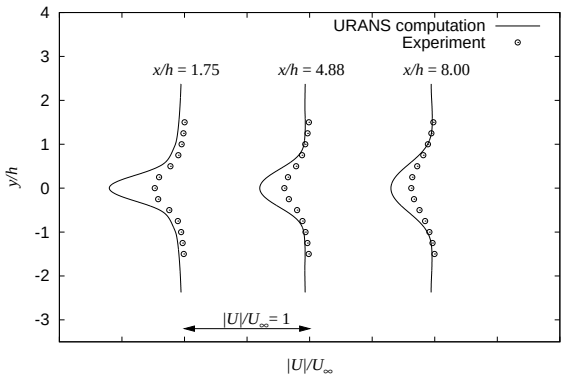

(c) PRNS

Figure 9: Comparison between time averaged URANS computation and experiment at various wake cross-sections